Journal of Radiological Science and Technology, 45(5), 397-405 ISSN 2384-1168(On-line) ISSN 2288-3509(Print)

<원저>

Baseline Correction in Computed Radiography Images with 1D Morphological Filter

Yong-Gwon Kim[1]·Yeunchul Ryu[2]

[1]Department of Radiological Science, Konyang University
[2]Department of Radiological Science, Gachon University

CR 영상에서 기저선 보정을 위한 1차원 모폴로지컬 필터의 이용에 관한 연구

김용권[1]·류연철[2]

[1]건양대학교 방사선학과·[2]가천대학교 방사선학과

Abstract Computed radiography (CR) systems, which convert an analog signal recorded on a cassette into a digital image, combine the characteristics of analog and digital imaging systems. Compared to digital radiography (DR) systems, CR systems have presented difficulties in evaluating system performance because of their lower detective quantum efficiency, their lower signal-to-noise ratio (SNR), and lower modulation transfer function (MTF). During the step of energy-storing and reading out, a baseline offset occurs in the edge area and makes low-frequency overestimation. The low-frequency offset component in the line spread function (LSF) critically affects the MTF and other image-analysis or qualification processes. In this study, we developed the method of baseline correction using mathematical morphology to determine the LSF and MTF of CR systems accurately. We presented a baseline correction that used a morphological filter to effectively remove the low-frequency offset from the LSF. We also tried an MTF evaluation of the CR system to demonstrate the effectiveness of the baseline correction. The MTF with a 3-pixel structuring element (SE) fluctuated since it overestimated the low-frequency component. This overestimation led the algorithm to over-compensate in the low-frequency region so that high-frequency components appeared relatively strong. The MTFs with between 11- and 15-pixel SEs showed little variation. Compared to spatial or frequency filtering that eliminated baseline effects in the edge spread function, our algorithm performed better at precisely locating the edge position and the averaged LSF was narrower.

Key Words: Morphological filter, Modulation transfer function, Baseline correction, Low frequency offset, Computed radiography
중심 단어: 모폴로지컬 필터, 변조전달 함수, 기저선 보정, 저주파수 옵셋, 컴퓨터 방사선촬영

Ⅰ. Introduction

The modulation transfer function (MTF) has been a common and useful performance indicator since the invention of film-based X-ray imaging systems[1-3]. In the era of digitalized X-ray imaging systems, the MTF is still used to evaluate the performance of systems or the quality of the digital images produced[4-6]. The MTF contains image resolution information as a function of spatial frequency[2] and it can indicate which system has better-resolving power by comparing the MTF profiles between systems. Because the MTF

This work was supported by the Gachon University research fund of 2015(GCU-2015-0062).
Corresponding author: Yeunchul Ryu, Department of Radiological Science, Gachon University, 191 Hambakmoe-ro, Yeonsu-gu, Incheon city, 21936, Republic of Korea / Tel: +82-32-820-4410 / E-mail: yeunchul.ryu@gachon.ac.kr
Received 20 June 2022; Revised 04 July 2022; Accepted 04 October 2022

describes the ability of an imaging system to transfer input modulations to output modulations at various spatial frequencies, the MTF can be mathematically derived from the Fourier amplitude of the point-spread function, which encodes a detector's response to an infinitely sharp impulse[7]. The MTF can be calculated from the line spread function (LSF) by Fourier transform[8], and the LSF is evaluated by differentiating the edge spread function (ESF).

For measuring an ESF of a detector, three methods are distinguished by the type of test object they use, bar pattern, slit, or edge[9]. Among these measurement methods, edge assessment is well-established for measuring the MTF and has also recently gained popularity for use in assessing the performance of digital X-ray systems. The edge-assessment method using a straight-edged object produces a better low-frequency response compared with the slit method[10]. The international standard for medical electrical equipment, IEC 62220-1[11], includes procedures for evaluating the characteristics of digital X-ray imaging devices. The diagram of an edge-test object included in Part 1 of that standard is reproduced in Fig. 1.

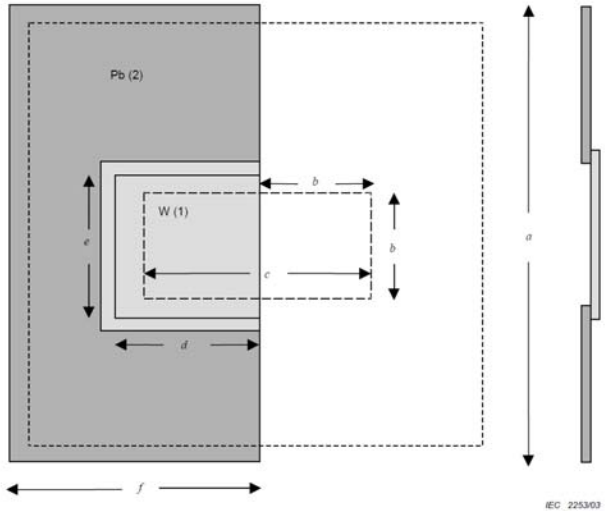

Fig. 1. Representative diagram of edge-testing equipment for CR (IEC 62220-1)

To determine the LSF and the MTF, edge assessment methods generally include the steps of image acquisition, edge detection, edge correction, and LSF-to-MTF conversion. However compared with digital radiography (DR) systems, relatively weak or low MTF characteristics of computed radiography (CR) system makes the assessment of a CR imaging system's performance with analytic methods harder[9,12,13]. In most low signal-to-noise ratio (SNR) X-ray imaging systems such as those using CR or indirect DR, edge algorithms that use a single-line profile yield inaccurate LSF results because they incorrectly estimate the edge position, which results in unsatisfactory MTF measurements[9]. Even with a corrected LSF reading, noise and low-frequency offsets from dispersing effects including scattering still affect the resulting MTF.

When X-rays impact the edge-testing device, some radiation is inevitably scattered. If the material is not thick enough to absorb all the radiation, the scattered radiation exits from the rear of the test object and travels toward the detector. In this case, the scattered radiation will be superimposed with the directly transmitted radiation that forms the image of the edge and will also weaken the attenuation of energy near the edge border. Thus, the X-ray profile at the detector surface differs from the desired step-shaped profile (see Fig. 2) like heel effects. Even more, the inaccuracy of CR digitizer makes low frequency component offset of latent image during the read processing[14]. Therefore, the measured ESF will differ from the target ESF and the determined MTF will not accurately represent the CR system's MTF[15].

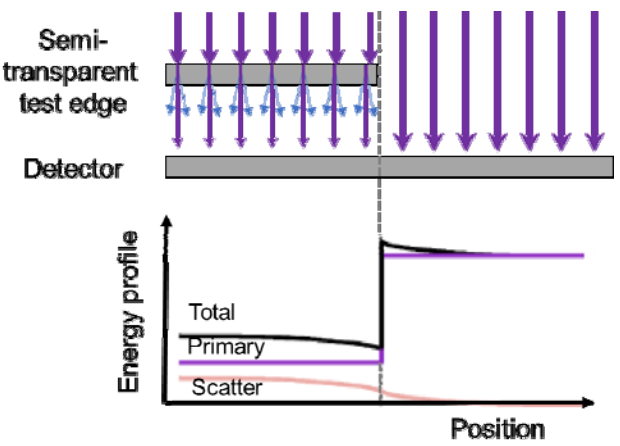

Fig. 2. Schematic distribution of the primary and scattered radiations for a semitransparent edge-testing sample [14]

The difficulty in removing these unwanted effects from the MTF with a single process lies in the fact that dispersing causes two quite different frequency components in the sampled profile. Scattered noise has high-frequency and randomly distributed features, while scattered radiation deposited on the transparent side of the edge has low-frequency and localized features. Standards such as IEC 62220-1 and other studies only consider noise elimination that uses spatial or frequency filters. However, the remaining low-frequency dispersing component leads these methods to overestimate performance and return incorrect dose calculations[17]. While comparing filtering methods in preliminary research for this study, we found that a morphological filter based on mathematical morphology theory performs well in efficiently eliminating both frequency components from scattering effects.

Therefore, the purpose of this study was to represent a method that can correct the dispersing effect using a morphological filter. We also report the effect of different structuring element (SE) sizes on the MTF measurements.

II. Materials and Methods

1. Configuration of the Imaging System and Edge Test

To acquire edge image data for the verification of the proposed algorithm, a CR X-ray imaging system (Progen 650R, Listem, Korea) was used. This system incorporates the imaging plate (IP) with dimensions of 24 × 30 cm (Kodak Carestream Health Inc., New York, USA) and a DIRECTVIEW Vita CR IP reader (Kodak Carestream Health Inc., New York, USA) with 2868 × 3460 pixel matrix and 86 μm pixel size. A 1.0-mm-thick tungsten plate affixed to a 3.0-mm-thick lead plate was placed on the IP and the region of interest (ROI) used for the measurement of the MTF was selected to include edge areas. The test apparatus was shown in our previous study[16]. In this study, we generally followed the IEC 62220-1 standard for assessing radiation specifications. The dimension of the ROI was selected as 1200 × 652 pixels. The length of the system from the source to the detector was 150 cm. The image was acquired with a tube voltage of 70 kVp and a tube current-exposure time product of 8 mAs.

2. Edge Algorithm Step

Fig. 3 shows a flow chart of the edge-detection algorithm for extracting MTF features from the image. In the edge detection and adjustment steps, we used Fourier shifts for LSF and ESF estimation[16]. These Fourier shifts allowed precise position corrections to the estimated edge that were calculated from the edge positions. The MTF could then be calculated from the LSF which was obtained by differentiating the ESF.

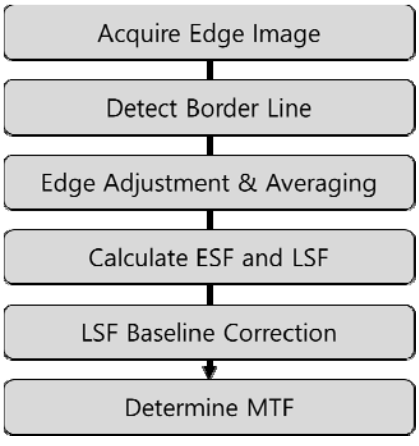

Fig. 3. Flow chart of the processing for an edge-detection algorithm

3. Baseline Correction with a Morphological Filter

In image processing, mathematical morphology theory allowed us to identify and extract meaningful image descriptors based on shapes within the image. Key applications of this theoretical tool were segmentation, automated counting, and inspection. Mathematical morphology encompassed a powerful and important body of methods, which could be precisely expressed within the framework of the set theory. Morphological operations could be applied to images of all types (1D, 2D, binary, gray-scale, full color, and others)[18,19].

However, their primary use was in processing binary data. The key morphological operators were dilation and erosion, and these were relatively simple to understand. The erosion of a binary image A by the SE B was defined as $A \ominus B = \{z \in E | B_z \subseteq A\}$, where Bz was the translation of B by the vector z. The dilation of A by the SE B was defined as $A \oplus B = \{z \in E | (B^s)_z \cap A \neq \Phi\}$, where Bz denoted a symmetric transformation of B. Many more sophisticated morphological operations (e.g.,opening, closing, and skeleton) could be reduced to a sequence of dilation and erosion operations[20].

To suppress the errors that resulted from scattering effects, our method estimated low-frequency components with a one-dimensional morphological filter and a cubic Hermite interpolator. To demonstrate the effects of SE size on the morphological filter, eight different SE sizes were applied to the opening operation (3-17 pixels at 2-pixel intervals). The opening operation was composed of two processing steps that performed erosion and dilation operations. A single operation was applied to the edge-adjusted LSF with a custom MATLAB program.

Ⅲ. Results

From the acquired edge image, we extracted a single-line profile along the middle horizontal, as shown in Fig. 4a, 4b[16]. The profile showed typical scattering effects around the edge, as well as the random noise distribution between the object edge and the transparent area. The horizontal axis of the ESF plot represented the pixel position from the origin of the ROI (bottom left) in units of pixels.

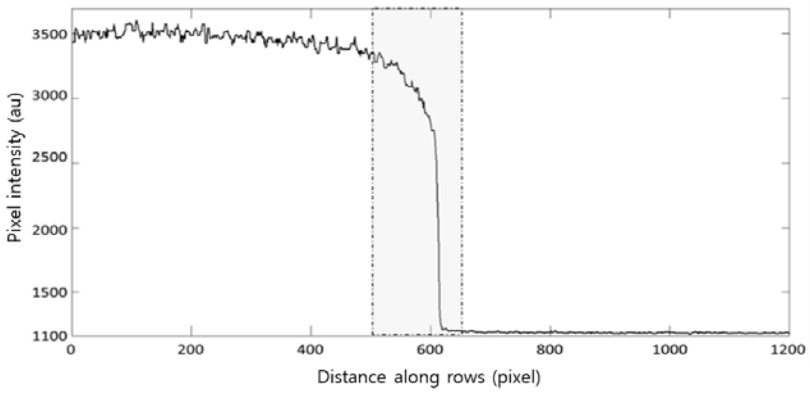

(a)

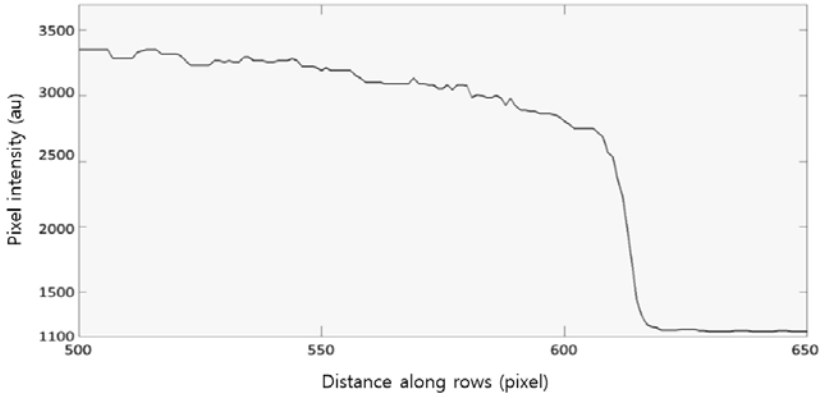

(b)

Fig. 4. The center-cropped ROI from an acquired image (courtesy of our previous study[16]). (a) Unprocessed horizontal-line profile. (b) Magnified plot of the gray region in (a)

The position-corrected LSF profiles were averaged into the single LSF profile shown in Fig. 5a[16]. The scattering effects around the edge remain in the averaged LSF. The position of the peak value represented the edge location. The amount of dispersing varied with the position. To the left side of the peak, the scattering effects gradually increase to a maximum near the edge but to the right side of the test object wherein X-rays should have passed through the air, the scattering effects occur around the edge although to a much smaller degree(Fig. 5a).

Fig. 5b shows the effect of applying averaging and a low-frequency offset in an MTF plot. When we used the single (non-averaged) profile, the calculated MTF curves included too much noise to estimate their exact high-frequency performance. And the averaged MTF was

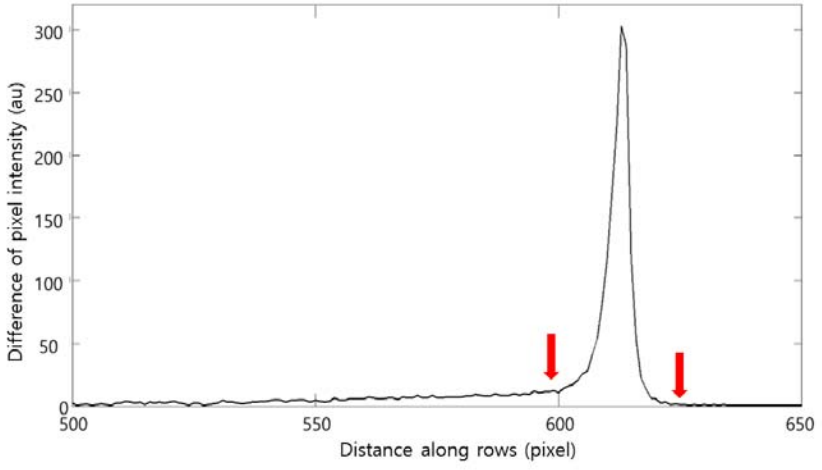

(a)

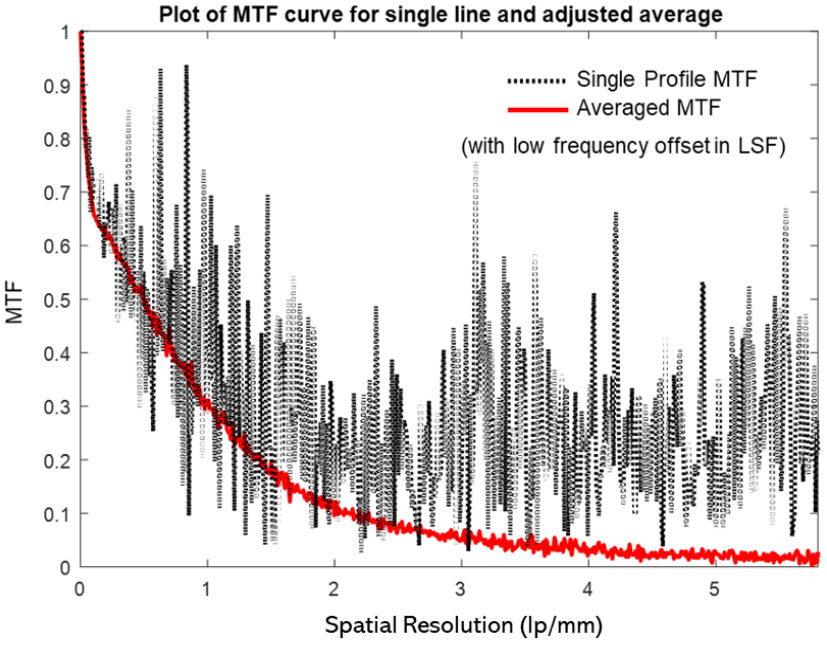

(b)

Fig. 5. LSF and MTF from averaged LSF profile. (a) The position-adjusted and averaged LSF profile of an acquired image (courtesy of our previous study[16]). In the magnified plot, the left and right sides of the maximum show different offset levels (marked with red arrows) (b) Plot with single-profile and averaged MTFs. The averaged MTF had a better SNR but still includes a strong peak near the low-frequency region due to the scattering offset

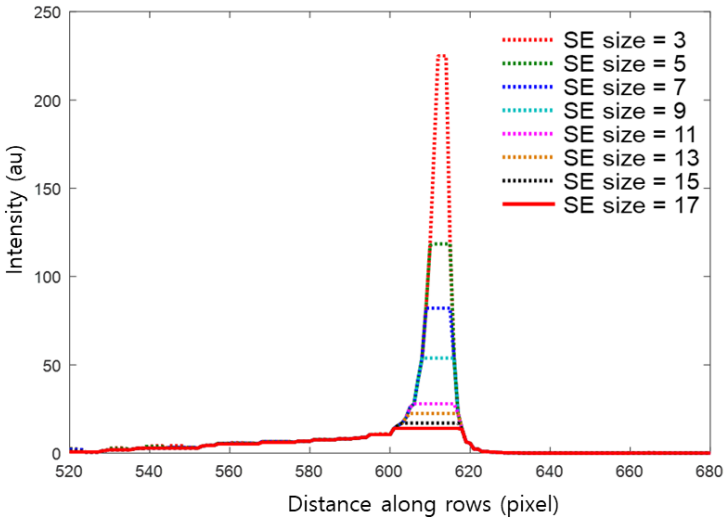

(a)

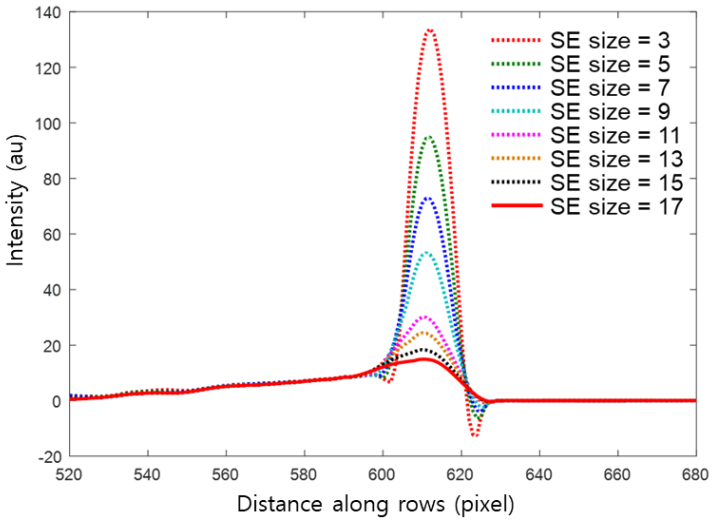

(b)

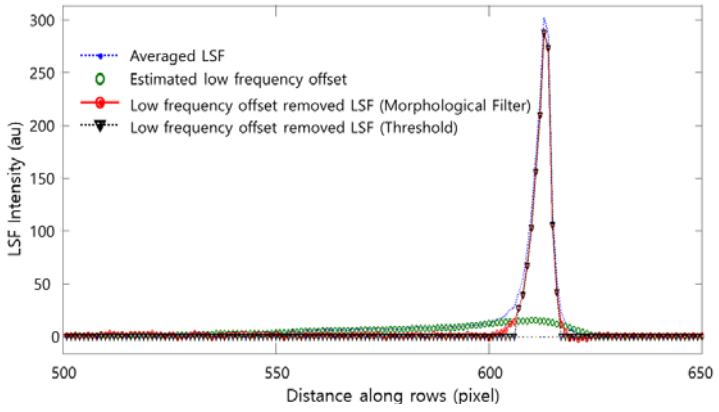

(c)

Fig. 6. The LSF profile (a) The LSF profile after the morphological opening operation. By increasing the size of SEs (3 to 17 pixels), the filtered LSF approached the known LSF (b) The cubic interpolation applied to the morphological filtered LSF (c) Elimination of the scattering effects from the measured LSF. The estimated low-frequency offset from morphological filtering and interpolation (green circle), and the final LSF from which the low-frequency component due to scattering effects have been removed

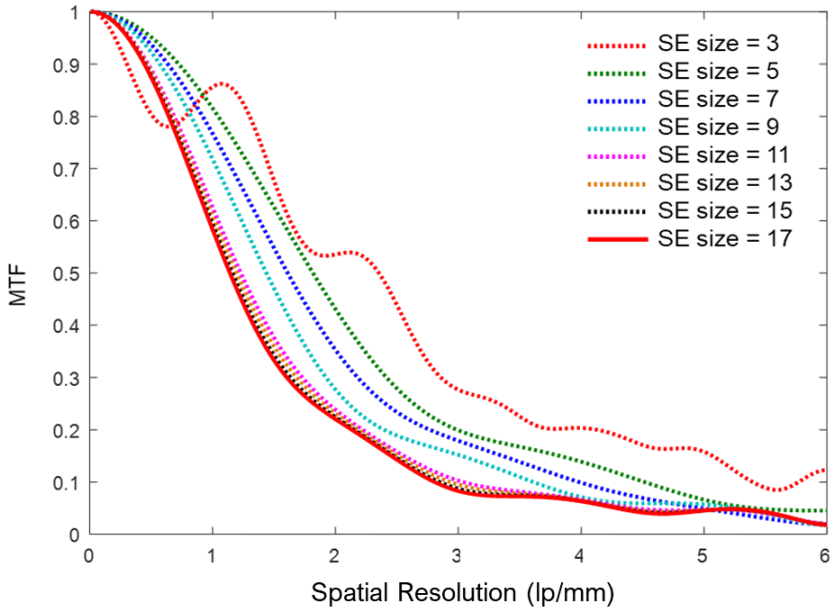

Fig. 7. Resultant MTF curves as different SE using proposed morphological filtering algorithm

shown in Fig. 5b with the red plot. But the low-frequency component of MTF was still overestimated.

The SE size indicated the closeness of the MTF curve to the acquired data. The effect of changing the SE size from 3 to 17 pixels was shown in Fig. 6a. For a SE size of 3 pixels, the remaining LSF profile was symmetrical but was just 3 pixels wide at the top. For a 17-pixel SE, the remaining LSF profile was asymmetric. For SE sizes from 11 to 17 pixels, the difference between the widths of the remaining profile was 6 pixels at maximum.

To reduce the discontinuity of filtered LSF, a cubic interpolator was applied to all filtered LSF profiles before calculating the MTF and its effect showed in Fig. 6b. This interpolation process corrected the discontinuity effect from the morphological filtering. In case of a 3-pixel SE, the resulting showed a maximal overestimated curve in dispersing offset area.

The elimination of the estimated low-frequency component was shown in Fig. 6c for a 15-pixel SE. The red line with circle markers was the final LSF and the green circles plot was the estimated offset of low-frequency dispersing effects. The LSF became symmetric around the edge and its peak value was very close to the given LSF profile. The intensity difference due to filtering at the edge was less than 9 pixels (3%) in this case.

The MTF curves were calculated by differentiation and normalization from the corrected LSF of Fig. 6c. The calculated MTF curves were shown in Fig. 7.

Ⅳ. Discussion

In this study, we extracted a single-line profile along the middle horizontal, as shown in Fig. 4a, 4b. In another study, the authors applied a dispersing effect removal step to the ESF[16], while in the present study, we applied the removal step to the LSF. This 1D morphological filtering step was preferred for detecting base components from spikes or peaks that were added to low-frequency data.

As we could see in Fig. 5b, if the single (non-averaged) profile was used, the MTF curves included too much noise and their high-frequency performance could not be determined. With averaged LSF profiles alone, however, the low-frequency components (at the left end of the MTF curve) were strong so that the profile did not precisely represent the performance of the CR system.

As 1D morphological processing was used to estimate

the scattering effects in this study, the SE size represented the area wherein the edge signal was dominant over the dispersing signal. The criterion for selecting this area was the symmetry of the remaining LSF profile after the morphological operations. As the morphologically filtered LSF was discontinuous, a cubic interpolator was applied to all filtered LSF profiles before calculating the MTF and its effect showed in Fig. 6b.

Fig. 7 shows Resultant MTF curves as different SE using the proposed morphological filtering algorithm. The elimination of scattering effects was more or less successful for different SE sizes. The MTF for processing with a 3-pixel SE fluctuated since it overestimated the low-frequency component. This overestimation led the algorithm to over-compensate in the low-frequency region so that high-frequency components appeared relatively strong. The MTFs for SE sizes from 11 to 17 pixels showed little variation since they estimate the low-frequency component similarly (see Fig. 6b). Compared with the method that eliminated scattering effects in the ESF, our algorithm performed better at precisely locating the edge position and the averaged LSF was narrower. The determination of optimal SE size depended on the resolving power of the imaging system as well as the exposure conditions of the X-ray source. In the present study, we optimized the SE size in the range of 11-15 pixels due to the experimental environments and the symmetry of the target LSF but the SE size could be optimized in different range for CR systems with various X-ray source conditions. In future research, we will evaluate the SNR or detective quantum efficiency of CR systems with similar algorithms by acquiring a broader range of data such as the noise power spectrum or detector uniformity.

V. Conclusions

This study developed a method for optimizable morphological filtering to eliminate low-frequency offsets while measuring the MTF of a CR system. With the proposed filtering methods, the baseline was clearly removed from the LSF. Our algorithm's robustness was demonstrated by correcting noise and dispersing effects using an edge phantom and a low-SNR CR system. The mathematical morphology algorithm precisely detected the target MTF without any additional filtering (such as a median-smoothing filter). Our easily implementable method could be extended to quality control for CR systems or for field use with a simple custom program for image post-processing.

REFERENCES

[1] Morgan RH, Bates LM, GapalaRao UV, Marinaro A. The frequency response characteristics of x-ray films and screens. Am. J. Roentgenol. 1964 Aug; 92(2):426-40.

[2] Rossmann K. Point spread-function, line spread-function, and modulation transfer function. Tools for the study of imaging systems. Radiology. 1969 Aug;93(2):257-72.

[3] Doi K, Bunch PC, Holje G, Pfeiler M, Wagner RF. Modulation transfer function of screen-film systems. IICRU Report 41. International Commission on Radiation Units and Measurements. Bethesda, Maryland; 1986.

[4] Sones RA, Barnes GT. A method to measure the MTF of digital x-ray systems. Med. Pys. 1984 Mar;11(2): 166-71.

[5] Hillen W, Schiebel U, Zaengel T. Imaging perform-ance of a digital storage phosphor system. Med. Phys. 1987 Mar;11(2):744-51.

[6] Morishita J, Doi K, Bollen R, Bunch PC, Hoeschen D, Sirandrey G, et al. Comparison of two methods for ac-curate measurement of modulation transfer functions of screen-film systems. Med. Phys. 1995 Feb;22(2):193-200.

[7] Barrett HH, Swindell W. Radiological imaging: The theory of image formation, detection, and processing. Elsevier Science: New York, USA; 1996.

[8] Bushberg JT, Seibert JA, Leidholdt EM, Boone JM. The essential physics of medical imaging. 3rd ed.

Lippincott Williams & Wilkins: A Wolters Kluwer Company; 2011.

[9] Samei E. Performance of digital radiographic detectors. In RSNA Categorical Course in Diagnostic Radiology Physics, Chicago, Illinois, USA; 2003.

[10] Cunningham IA, Reid BK. Signal and noise in modulation transfer function determinations using the slit, wire, and edge techniques. Med. Phys. 1992 Jul;19(4):1037-44.

[11] International electrotechnical commission, international standard IEC62220-1: Medical electrical equipment-Characteristics of digital imaging devices-Part 1: Determination of the detective quantum efficiency: IEC; 2003.

[12] Min JW, Kim JM, Jeong HW. Mixed noise reduction filters for CR Images. Journal of Radiological Science and Technology. 2007 Mar;30(1):1-6.

[13] Jeong HW, Min JW, Kim JM, et al. Investigation of Physical Imaging Properties in Various Digital Radiography System. Journal of Radiological Science and Technology. 2017;40(3):363-70.

[14] Neitzel U, Buhr E, Hilgers G, Granfors PR. Determination of the modulation transfer function using the edge method: Influence of scattered radiation. Med. Phys. 2004 Dec;31(12):3485-91.

[15] Shetty CM, Barthur A, Kambadakone A, Narayanan N, Kv R. Computed Radiography Image Artifacts Revisited. AJR. 2011;196:W37-47.

[16] Kim YG, Ryu Y. Accurate evaluation of modulation transfer function using the Fourier shift theorem. J. Korean Phys. Soc. 2017 Sep;71(12):1064-8.

[17] Mackenzie A, Workman A, Dance DR, Yip M, Wells K, Young KC. Validation of a method to convert an image to appear as if acquired using a different digital detector. Proc. SPIE 7961, 2011 Mar 16;Lake Buena Vista, Florida (United States):SPIE;c2011. 79614F.

[18] Maragos P, Schafer R. Morphological filters-Part I: Set-theoretic analysis. In Proceedings of IEEE Transactions on Acoustics Speech and Signal. 1987 Aug;35(8):1153-69.

[19] Maragos P, Schafer R. Morphological filters-Part II: Their relations to median, order-statistic, and stack filters. In Proceedings of IEEE Transactions on Acoustics Speech and Signal. 1987 Aug;35(8):1170-84.

[20] Solomon C, Breckon T. Fundamentals of digital image processing. WILEY-BLACKWELL: John Wiley & Sons, Ltd; 2011:197-232.

구분	성명	소속	직위
제1저자	김용권	건양대학교 방사선학과	부교수
교신저자	류연철	가천대학교 방사선학과	부교수